

# A Wavelength Tunable CW Orange-red Laser Source Based on Magnesium Oxide-doped Periodically-poled LiNbO<sub>3</sub> in an Intracavity Sum-frequency Generation

Yang BAI<sup>1\*</sup>, Jianlin LI<sup>1,2</sup>, Guangzhi LEI<sup>2</sup>, Lei HOU<sup>1</sup>, Rongwei ZHA<sup>1</sup>, Yi WANG<sup>1</sup>, Haowei CHEN<sup>1</sup>

<sup>1</sup>National Key Laboratory of Photoelectric Technology and Functional Materials (Culture Base), Institute of Photonics and Photon-Technology, Northwest University, Xi'an 710075, P. R. China

<sup>2</sup>Space Optical Technology Research Department, Xi'an Institute of Optics and Precision Mechanics of CAS, Xi'an 710119, P. R. China

**crossref** <http://dx.doi.org/10.5755/j01.ms.26.4.22640>

Received 28 January 2019; accepted 05 April 2019

A watt-level continuous wave (CW) orange-red laser with wavelength tunable properties is experimentally implemented based on sum-frequency generation (SFG) in a composite cavity. The cavity is composed of an 880 nm laser diode (LD) side-pumped Nd: GdVO<sub>4</sub> *p*-polarized 1062.9 nm cavity and a single-resonant optical parametric oscillator (SRO) of signal light using a magnesium oxide-doped periodically-poled LiNbO<sub>3</sub> (MgO: PPLN) crystal with a poling period of 29.1 μm. In the overlap region of the two cavities, orange-red laser is generated by using a type-II critical phase-matched potassium titanyl phosphate crystal (KTP) crystal. In the temperature tuning range of the MgO: PPLN crystal (from 30 °C to 200 °C), the CW orange-red laser beams are generated in a tunable waveband from 612.24 nm to 620.72 nm ( $\Delta\lambda = 8.48$  nm), corresponding to the mid-infrared idler light is also obtained with tunable wavelength from 4027.5 nm to 3708.2 nm ( $\Delta\lambda = 319.3$  nm). At the lowest tuning temperature of 30 °C, the maximum CW output power of the orange-red laser at 612.24 nm and the idler light at 4027.5 nm are obtained, which are 1.145 W and 2.83 W, respectively.

**Keywords:** wavelength tuning, orange-red laser, composite cavity, signal SRO, intracavity SFG.

## 1. INTRODUCTION

High power orange-red lasers in the 600–650 nm region are strongly desirable visible laser sources can be utilized in such important applications as spectral analysis, biomedicine, optical pumping, and laser projection displays etc [1–3]. Conventionally, high power orange-red lasers can be realized by intracavity sum-frequency generation (SFG) via various approaches, such as laser diode (LD) pumped Nd<sup>3+</sup>-doped crystals [4, 5], Pr<sup>3+</sup>-doped crystals pumped by the intracavity frequency doubled Nd<sup>3+</sup> laser [6, 7], GaInNAs/GaAs semiconductor disk laser based second-harmonic generation (SHG) [8, 9], or Raman frequency shift technology [10, 11]. However, such lasers usually output a single wavelength, which is not satisfied to the applications where wide band wavelength is required. Recently, orange-red laser with tunable wavelength has been demonstrated by using an optical parametric oscillation (OPO) through pump laser and signal light in the intracavity SFG process [12–14]. However, in the above report, the difficulty of the method is greatly increased when the device is aligned to achieve synchronous phase matching of two nonlinear frequency conversion processes in one periodically-poled crystal. The pump laser acts as pump laser for the OPOs and fundamental laser for the SFG process. Therefore, the double functions of the pump laser force the output power

is dispersed to two nonlinear frequency conversion processes, and finally lead to a low power continuous wave (CW) output of wavelength tunable orange-red laser.

Here, we demonstrate a wavelength tunable orange-red laser source with a tunable waveband from 612.24 nm to 620.72 nm, which has a compound cavity structure consisting of a *p*-polarized CW 1062.9 nm fundamental frequency laser and a single-resonant optical parametric oscillator (SRO) using a magnesium oxide-doped periodically-poled LiNbO<sub>3</sub> (MgO: PPLN) crystal. The wavelength tunable orange-red laser is realized through the intracavity-SFG of the two independently oscillating laser beams mentioned above. The ABCD matrix theory is used to design and optimize the structure parameters of the compound cavity, in order to make the mode volume matching between the signal light and the 1062.9 nm fundamental frequency laser better. Our results show potential application of the composite cavity structure based on the SRO and intracavity-SFG on designing orange-red laser with high CW power and tunable wavelength.

## 2. EXPERIMENTAL SETUP

The wavelength tunable orange-red laser system was designed as a composite cavity structure. The experimental setup is schematically illustrated in Fig. 1. The composite cavity contains three main components: a cavity of *p*-polarized 1062.9 nm fundamental frequency laser, an *s*-polarized signal SRO based on quasi-phase-matching

\* Corresponding author. Tel.: +86-029-88303781.  
E-mail address: [by@nwu.edu.cn](mailto:by@nwu.edu.cn) (Y. Bai)

$1/\lambda_s$ -polarized pump  $\rightarrow 1/\lambda_s$ -polarized signal +  $1/\lambda_s$ -polarized idler [15] and its pump source.

The pump source of the  $s$ -polarized signal SRO is an  $s$ -polarized 1062.9 nm laser with a linewidth (full width at half maximum of the spectral line type measured by the experiment, referred to as FWHM) of  $\sim 0.3$  nm. It is formed by a plane mirror  $M_1$  (reflectivity:  $R > 99.9\%$  at  $s$ -polarized 1062.9 nm), a 880 nm-LD side pumped module-1 (880 nm-LDSPM-1), and a planar output coupler  $M_2$  with a transmittance of 15% at  $s$ -polarized 1062.9 nm. A 0.5 at.%  $\text{Nd}^{3+}$  doped Nd:  $\text{GdVO}_4$  crystal rod ( $\Phi 2 \times 65$  mm rod) was used as the gain medium, which was side pumped by three 880 nm LD arrays and water cooled to 20 °C. The diode pump wavelengths that have been used effectively with Nd:vanadate crystals include 808 nm, 880 nm, and 888 nm [16]. The pumping absorption at 888 nm of Nd:vanadate crystals is very weak compared with that at 808 nm and 880 nm [16, 17]. The effective absorption cross sections of Nd:  $\text{GdVO}_4$  crystal at 808 nm and 880 nm were  $5.2 \times 10^{-19} \text{ cm}^2$  and  $2.7 \times 10^{-19} \text{ cm}^2$  [18], respectively. Compared to 808 nm pumping, which populates the  $^4F_{5/2}$  level of Neodymium, pumping at 880 nm populates the upper laser level  $^4F_{3/2}$  directly, leading to important benefits of lower quantum deficiency and weaker absorption coefficient, alleviating thermal loading. Therefore, the 880 nm laser diode acts as a pump source, which can reduce quantum losses and radically reduce the thermal load generated in the laser crystal [18–20]. Thereby, the thermal effect in laser crystal can be partially alleviated, and the output power and beam quality can be improved. The Maximum total pump power of the 880 nm LD arrays is 70 W. The 1064 nm fundamental frequency laser produced by stimulated radiation of the Nd:  $\text{GdVO}_4$  crystal has high polarization properties [21, 22]. Therefore, the polarization direction of the 1062.9 nm fundamental frequency laser is rotated by two 1/2 waveplates were rotated in order to meet the type-II phase matching condition of the two polarization states ( $s$ -polarized form or the  $p$ -polarized form) in the SFG process [18].

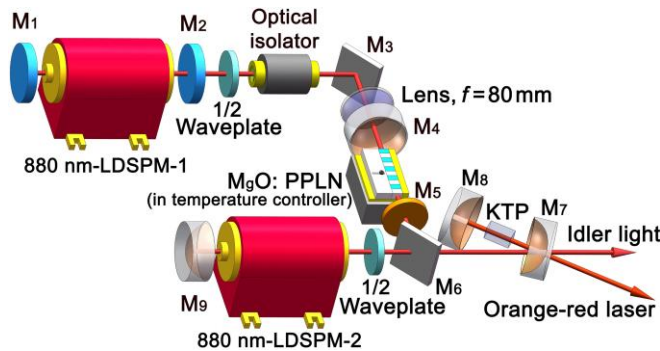


**Fig. 1.** Diagram of the experimental setup

The  $s$ -polarized signal SRO including mirrors  $M_4$ ,  $M_5$ ,  $M_6$ ,  $M_7$ ,  $M_8$  and a MgO: PPLN crystal with a grating period of 29.1  $\mu\text{m}$  forms a U-type cavity. Between the mirrors  $M_4$  and  $M_5$ , the MgO: PPLN crystal ( $50 \times 3 \times 1 \text{ mm}^3$ , MgO doping concentration of 5 mol %) was placed in a high precision temperature controller with a precise temperature control range from 30 °C to 200 °C

(Exceeding this range, the control accuracy of the temperature furnace will be greatly reduced, resulting in large fluctuations in the center wavelengths of the signal light and the idler light), its two end surfaces were anti-reflection (AR) coated for the pump laser ( $R < 5\%$  at 1062.9 nm), signal light ( $R < 5\%$  at 1410–1510 nm) and idler light ( $R < 5\%$  at 3650–4100 nm). The fine tuning of the A 1/2 waveplate ensures that the polarization of the pump laser was still  $s$ -polarized after passing through the lens with 80 mm focal length. The incident face of the plane-concave mirror  $M_4$  was AR coated for the pump laser ( $R < 2\%$  at 1062.9 nm), and its concave side was HR coated for the signal light ( $R > 99.5\%$  at 1410–1510 nm) and idler light ( $R > 96.5\%$  at 3650–4100 nm). Mirror  $M_5$  is a plane harmonic beam splitting mirror. It was HR coated for the pump laser ( $R > 98\%$  at 1062.9 nm) on the side close to the MgO: PPLN crystal and AR coated for the signal light ( $R < 1\%$  at 1410–1510 nm) and idler light ( $R < 3.5\%$  at 3650–4100 nm) on the other side.

The reflection of the pump laser at 1062.9 nm can improve the conversion efficiency of the SRO, but this may also cause damage to the 880 nm-LDSPM-1. Therefore, in order to protect the 880 nm-LDSPM-1, it is necessary to insert a high power polarization-dependent optical isolator (at 1064 nm center wavelength, 85 W maximum input power and 7 mm maximum beam diameter) between the 1/2 waveplate and mirror  $M_3$ . The plane mirror  $M_6$  was HR coated on the side close to the mirror  $M_5$  for the signal light ( $R > 99.3\%$  at 1410–1510 nm) and idler light ( $R > 97.8\%$  at 3650–4100 nm), and coated 45° incident-AR for the fundamental frequency laser ( $R < 1.5\%$  at 1062.9 nm). The other face was coated 45° incident-AR for the fundamental frequency laser ( $R < 0.5\%$  at 1062.9 nm). The plane-concave mirror  $M_7$  was used as an output coupling mirror. Its concave side was coated 15° incident-HR for the signal light ( $R > 99.5\%$  at 1410–1510 nm) and fundamental frequency laser ( $R > 99.5\%$  at 1062.9 nm), and 15° incident-AR for the orange-red laser ( $R < 3\%$  at 600–630 nm) and idler light ( $R < 10\%$  at 3650–4100 nm). The plane-concave  $M_8$  was HR coated for the fundamental frequency laser ( $R > 99.6\%$  at 1062.9 nm), signal light ( $R > 99.6\%$  at 1410–1510 nm), and orange-red laser ( $R > 99\%$  at 600–630 nm). As shown in Fig. 1, a V-type cavity of fundamental frequency laser at the  $p$ -polarized 1062.9 nm was configured by a plane-concave mirror  $M_9$ , a 880 nm-LD side pumped module-2 (880 nm-LDSPM-2, it is identical to 880 nm-LDSPM-1), a 1/2 waveplate,  $M_6$ ,  $M_7$  and  $M_8$ , respectively. The concave side of  $M_9$  was HR coated for the fundamental frequency laser ( $R > 99.8\%$  at 1062.9 nm). Between mirrors  $M_7$  and  $M_8$ , a critical phase-matched type-II KTP crystal with dimension of  $5 \times 5 \times 7 \text{ mm}^3$  ( $\theta = 68.5^\circ$ ,  $\phi = 0^\circ$ ) was placed in the beam waist overlapped region of the signal light ( $s$ -polarized) and fundamental frequency laser ( $p$ -polarized) to generate  $p$ -polarized orange-red laser through SFG ( $1/\lambda_p$ -polarized orange-red  $\rightarrow 1/\lambda_s$ -polarized signal +  $1/\lambda_p$ -polarized 1062.9 nm). Its two faces were AR coated for the fundamental frequency laser ( $R < 99.5\%$  at 1062.9 nm), signal light ( $R < 99.5\%$  at 1410–1510 nm), and orange-red laser ( $R < 1.5\%$  at 600–630 nm), respectively.

### 3. OPTIMIZATION OF CAVITY PARAMETERS

Obviously, the off-axis placed plane-concave mirrors in folded cavities will cause the astigmatism and the thermal focal length of the fundamental frequency laser ( $p$ -polarized) and signal light ( $s$ -polarized) to be different, thereby causing the mode volume of the two light beams to be mismatched and their beam waists cannot achieve effective overlap in the type-II KTP crystal. Therefore, the conversion efficiency of orange-red laser will not be further improved by SFG method [23]. Here, ABCD matrix theory is employed to design and optimize the cavity parameters by using the laser cavity analysis and design software (LASCAD). In the numerical simulation process, the curvature radius of  $M_4$ ,  $M_7$ ,  $M_8$  and  $M_9$  were defined as 1000 mm, 200 mm, 100 mm and 1000 mm, respectively. The length of the signal SRO is  $\sim 400$  mm. Among them, the distances between adjacent two optical elements in  $M_4$ , MgO: PPLN crystal,  $M_5$ ,  $M_6$ ,  $M_7$ , and  $M_8$  are 26 mm, 4 mm, 45 mm, 142 mm, 77 mm and 49 mm, respectively. The cavity length of the  $p$ -polarized 1062.9 nm fundamental frequency light was the same as that of the signal SRO. The distances between  $M_9$  and Nd: GdVO<sub>4</sub> crystal and between Nd: GdVO<sub>4</sub> crystal and  $M_6$  are 30 mm. As shown in Fig. 2, we can observe how the spot sizes of the  $p$ -polarized 1062.9 nm fundamental frequency light and  $s$ -polarized signal light change along the cavity. The radii of the fundamental frequency light and signal light are approximately constants. This result indicates that the astigmatism of the folded composite cavity was compensated. The radii of the  $s$ -polarized signal light and the  $p$ -polarized 1062.9 nm fundamental frequency light in the KTP crystal were calculated to be  $\sim 150 \mu\text{m}$ , respectively. An optimum model volume matching could reduce the diffraction loss, lower the threshold and improve the conversion efficiency of the intracavity-SFG.

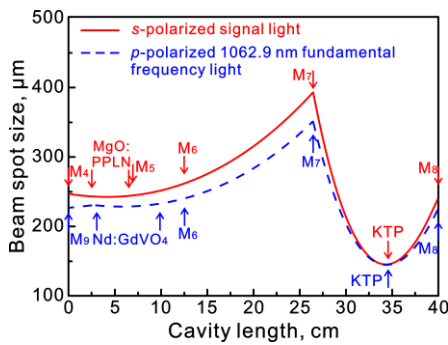


**Fig. 2.** Simulated curves of spot size variation of  $s$ -polarized signal light and  $p$ -polarized 1062.9 nm fundamental frequency laser along the cavity

### 4. EXPERIMENTAL RESULTS AND DISCUSSION

Temperature control of the MgO: PPLN crystal enables the tunable spectra for the idler light, as shown in the inset in Fig. 3 a. When the temperature was increased from 30 °C to 200 °C, the measured center wavelength of the idler light blue shifted from 4027.5 nm using a grating spectrometer equipped with a liquid-nitrogen-cooled InSb detector (Omni- $\lambda$ 7515, wavelength range: 400 nm–5.0  $\mu\text{m}$ , resolution:

0.01 nm@400 nm–1.0  $\mu\text{m}$  and 0.1 nm@1.0  $\mu\text{m}$ –5.0  $\mu\text{m}$ , Beijing Zolix Instruments Co., Ltd), showing a tuning range of 319.3 nm. The linewidth of the idler lights was measured to be  $\sim 15$  nm. The corresponding theoretical center wavelength of the signal light was from 1443.98 nm to 1489.98 nm. The center wavelength of the idler light was shifted toward the long wavelength direction with the tuning temperature increasing of MgO: PPLN crystal. Meanwhile, the thermal effect and phase mismatch of MgO: PPLN crystal were increased. This phenomenon caused the maximum CW output power of the idler light and the maximum intracavity power density of the signal light were decreased with the increase of the tuning temperature or the pump power of the 880 nm-LDSPM-1, as shown in Fig. 3 a. Fig. 3 b shows that the CW output power of the idler light was increased approximately linearly with the increase of pump power of the 880 nm-LD side pump module-1 at four different tuning temperatures of 30 °C, 90 °C, 150 °C and 200 °C, respectively. From 30 °C to 200 °C, the center wavelengths of the idler lights corresponding to the four temperature points were 4027.5 nm, 3917.3 nm, 3814.2 nm and 3708.2 nm, respectively.

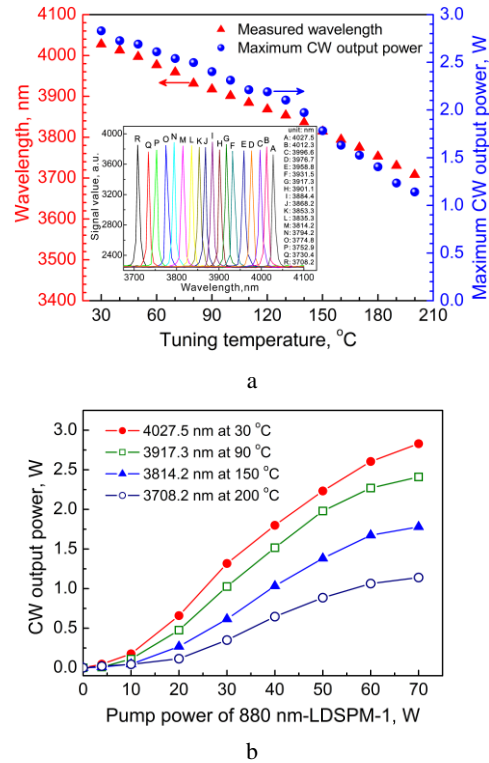


**Fig. 3.** a–center wavelengths and maximum CW output powers of idler lights as a function of the temperature tuning range from 30 °C to 200 °C; b–CW output powers variation of idler lights with pump power of 880 nm-LDSPM-1 at and four tuning temperatures of 30 °C, 90 °C, 150 °C and 200 °C

Their maximum CW output powers were 2.83 W, 2.41 W, 1.78 W and 1.14 W measured by using a laser power probe (S415C, wavelength range: 190 nm–20  $\mu\text{m}$ , resolution: 100  $\mu\text{W}$ , Thorlabs Co., Ltd), respectively, and the corresponding optical-to-optical (880 nm LD to idler light) conversion efficiencies were 4.04 %, 3.44 %, 2.54 % and 1.63 %, respectively. In 20 minutes, the CW power

was measured in 10 seconds time step. The power instabilities of the idler lights were calculated as  $\pm 2.27\%$ ,  $\pm 2.64\%$ ,  $\pm 3.08\%$  and  $\pm 3.57\%$ , respectively, identifying a good stability of the proposed composite cavity.

In the SFG process, the gain matching principle must be followed (i.e., the photon ratio of the 1062.9 nm fundamental frequency laser and the optical signal is 1: 1). However, the maximum intracavity power density of the signal light was decreased with the increase of the tuning temperature. Therefore, the pump power of the 880 nm-LDSPM-2 was adjusted with the change of tuning temperature. This ensures that the optimum intracavity power density of the 1062.9 nm fundamental frequency laser was matched with the maximum intracavity power density of the signal light at a fixed temperature. By this method, the maximum output power of the orange-red laser was easily obtained.

At 70.0 W maximum pump power of the 880 nm-LDSPM-1, the characteristics of the center wavelength and maximum CW output power for the orange-red laser were presented in Fig. 4 a, as the tuning temperature was tuned from 30 °C to 200 °C. It should be noted that the measured center wavelength of the orange-red laser slightly red shifts compared to the theoretical value by formula  $\lambda_{\text{orange-red}} = (\lambda_{\text{signal}} - \lambda_{1062.9 \text{ nm}}) / (\lambda_{\text{signal}} + \lambda_{1062.9 \text{ nm}})$ .

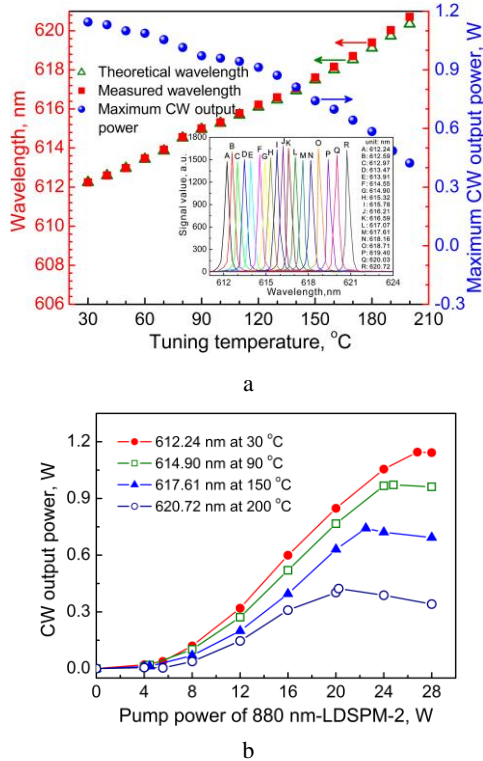


**Fig. 4.** a—center wavelengths and maximum CW output powers of the orange-red laser as a function of the temperature tuning range from 30 °C to 200 °C; b—CW output powers variation of the orange-red laser with pump power of 880 nm-LDSPM-2 at and four tuning temperatures of 30 °C, 90 °C, 150 °C and 200 °C

This can be attributed to stimulated Raman scattering red-shift in the MgO: PPLN crystal [24] when the intracavity power density is high. As expected, the maximum CW output power of the orange-red laser also

exhibits decreases linearly with increasing tuning temperature, which is due to the decrease in the maximum intracavity photon number of the *s*-polarized signal light with increasing tuning temperature. When 880 nm-LDSPM-1 worked at the maximum value of 70.0 W, the output power characteristics of the orange-red laser as the function of the 880 nm-LDSPM-2 pump power was presented in Fig. 4 b at different tuning temperatures of 30 °C, 90 °C, 150 °C and 200 °C, respectively. When the pump power of the 880 nm-LDSPM-2 for producing the *p*-polarized 1062.9 nm laser continuously increased, the CW output power of the orange-red laser was appear saturated due to the more serious thermal effect and the saturation of the *s*-polarized signal light photon number in the cavity. And as the tuning temperature increased, the saturation of the laser output power became more apparent. In addition, it needs to be explained that the central wavelength change of the signal light in our experiment caused a slight error between the best phase matching angle of the SFG process and the fixed phase matching angle of the type-II KTP crystal. This also somewhat affected the CW output power of the orange-red laser to further increase. The measured center wavelengths of the orange-red laser beams were 612.24 nm, 614.90 nm, 617.61 nm, and 620.72 nm, respectively, which in turn correspond to four temperature points of 30 °C, 90 °C, 150 °C, and 200 °C. From 30 °C to 200 °C, the maximum CW output power of 1.145 W, 0.972 W, 0.742 W, and 0.423 W was obtained when the pumping power of the 880 nm-LDSPM-2 was 26.8 W, 24.7 W, 22.5 W and 20.2 W, respectively. The corresponding total optical-to-optical (880 nm LD to orange-red laser) conversion efficiencies were about 1.18 %, 1.02 %, 0.80 %, and 0.47 %, respectively. In addition, the power instability of the orange-red laser beam in 20 minutes was calculated as  $\pm 2.31\%$ ,  $\pm 2.68\%$ ,  $\pm 3.12\%$  and  $\pm 3.63\%$ , respectively, giving a comparable stability performance to the corresponding idler light.

Additionally, using a laser beam quality analyzer without power attenuation (ModeScan1740, Photon USA Inc.), the beam quality factors  $M^2$  of the orange-red laser at 612.24 nm and 620.72 nm were measured as  $M_x^2$  and  $M_y^2$  of (4.1, 4.7) and (4.8, 5.1), corresponding to the tuning temperature 30 °C and 200 °C, respectively. The real spot photos taken by the camera, the 2D and 3D near field beam profiles of the orange-red laser beams are shown in Fig. 5.

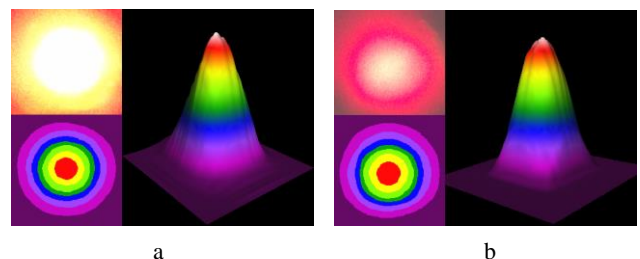


**Fig. 5.** Real spot photos taken by the camera, 2D and 3D near field beam profiles of the orange-red laser at: a—612.24 nm; b—620.72 nm

The results show that the orange-red laser beams had a good Gauss distribution because the astigmatism of the folded cavity is compensated. The elliptical spots were the

consequence of spatial walk-off in type-II critical phase-matched KTP crystal.

## 5. CONCLUSIONS

In conclusion, we have reported a wavelength tunable orange-red laser source with a tunable waveband from 612.24 nm to 620.72 nm ( $\Delta\lambda = 8.48$  nm) and a CW output power up to watt level. The laser source was also capable of outputting a multi-watt level wavelength tunable CW mid-infrared laser with a tunable waveband from 4027.5 nm to 3708.2 nm ( $\Delta\lambda = 319.3$  nm). We have shown experimentally that by taking advantage of the composite cavity, MgO:PPLN crystal temperature tuning and intracavity-SHG, a wavelength tunable high power CW orange-red laser could be constructed. The simple, compact and wavelength tunable orange-red laser with flexible outputs can meet many potential applications such as biomedicine, laser measurement, laser displays, spectral analysis, etc.

## Acknowledgments

This work was financially supported by National Key Research and Development Program of China (2017YFB0405102).

## REFERENCES

1. **Bernstein, E.F., Bhawalkar, J., Clifford, J., White, J., Hsia, J.** Laser Treatment of Dyschromia With a Novel 607 nm Pulsed-Dye Laser *Journal of Drugs in Dermatology: JDD* 10 (4) 2011: pp. 388–394.  
<https://jddonline.com/articles/dermatology/S1545961611P0388X/1>
2. **Alford, W.J., Fetzer, G.J., Epstein, R.J., Sandalphon, A., Lieu, N.V., Ranta, S., Tavast, M., Leinonen, T., Guina, M.** Optically Pumped Semiconductor Lasers for Precision Spectroscopic Applications *IEEE Journal of Quantum Electronics* 49 (8) 2013: pp. 719–727.  
<https://doi.org/10.1109/JQE.2013.2270912>
3. **Majid, M.A., Al-Jabr, A.A., Oubei, H.M., Alias, M.S., Anjum, D.H., Ng, T.K., Ooi, B.S.** First Demonstration of InGaP/InAlGaP Based Orange Laser Emitting at 608 nm *Electronics Letters* 54 (14) 2015: pp. 1102–1104.  
<https://doi.org/10.1049/el.2015.1658>
4. **Yu, X., Sun, G.C., Li, B.Z., Zhang, X.H., Jin, G.Y.** All-solid-state CW Doubly Resonant Sum-frequency Mixing Red-orange Laser at 611 nm *Laser Physics* 21 (6) 2011: pp. 1057–1060.  
<https://doi.org/10.1134/S1054660X11110375>
5. **Li, B.Z., Su, X.X., Guo, L.J., Lin, J.Q., Gao, X., Li, X.K., Zhang, X.H., Sun, G.C.** Diode-pumped Nd:YAP Sum-Frequency Mixing Orange-red Laser at 616 nm *Laser Physics* 21 (6) 2011: pp. 1061–1063.  
<https://doi.org/10.1134/S1054660X11110168>
6. **Luo, S.Y., Yan, X.G., Cui, Q., Xu, B., Xu, H.Y., Cai, Z.P.** Power Scaling of Blue-diode-pumped Pr: YLF Lasers at 523.0, 604.1, 606.9, 639.4, 697.8 and 720.9 nm *Optics Communications* 380 2016: pp. 357–360.  
<https://doi.org/10.1016/j.optcom.2016.06.026>
7. **Metz, P.W., Marzahl, D.T., Guguschev, C., Bertram, R., Kränkel, C., Huber, G.** Growth and Diode-pumped Laser Operation of Pr<sup>3+</sup>:  $\beta$ -(Y<sub>0.5</sub>, Gd<sub>0.5</sub>)F<sub>3</sub> at Various Transitions *Optics Letters* 40 (12) 2015: pp. 2699–2702.  
<https://doi.org/10.1364/OL.40.002699>
8. **Konttinen, J., Korpjärvi, V.M.** Frequency-converted Dilute Nitride Laser Diodes for Mobile Display Applications *Nanoscale Research Letters* 9 (1) 2014: pp. 1–5.  
<https://doi.org/10.1186/1556-276X-9-82>
9. **Kantola, E., Leinonen, T., Penttinen, J.P., Korpjärvi, V.M., Guina, M.** 615 nm GaInNAs VECSEL with Output Power Above 10 W *Optics Express* 23 (16) 2015: pp. 20280–20287.  
<https://doi.org/10.1364/OE.23.020280>
10. **Lee, A.J., Lin, J.P., Pask, H.M.** Near-infrared and Orange-red Emission from a Continuous-wave, Second-Stokes Self-Raman Nd: GdVO<sub>4</sub> laser *Optics Letters* 35 (18) 2010: pp. 3000–3002.  
<https://doi.org/10.1364/OL.35.003000>
11. **Kablukov, S.I., Babin, S.A., Churkin, D.V., Denisov, A.V., Kharenko, D.S.** Frequency Doubling of a Raman Fiber Laser *Laser Physics* 20 (2) 2010: pp. 365–371.  
<https://doi.org/10.1134/S1054660X10030096>
12. **Fedorova, K.A., Sokolovskii, G.S., Nikitichev, D.I., Battle, P.R., Krestnikov, I.L., Livshits, D.A., Rafailov, E. U.** Orange-to-red Tunable Picosecond Pulses by Frequency Doubling in a Diode-pumped PPKTP Waveguide *Optics Letters* 38 (15) 2013: pp. 2835–2837.  
<https://doi.org/10.1364/OL.38.002835>
13. **Mieth, S., Henderson, A., Halfmann, T.** Tunable, Continuous-wave Optical Parametric Oscillator with More than 1W Output Power in the Orange Visible Spectrum *Optics Express* 22 (9) 2014: pp. 11182–11191.  
<https://doi.org/10.1364/OE.22.011182>
14. **Fedorova, K.A., Sokolovskii, G.S., Battle, P.R., Livshits, D.A., Rafailov, E.U.** 574–647 nm Wavelength Tuning by Second-harmonic Generation from Diode-pumped PPKTP Waveguides *Optics Letters* 40 (5) 2015: pp. 835–838.  
<https://doi.org/10.1364/OL.40.000835>
15. **Sheng, Q., Ding, X., Yin, S.J., Shi, C.P., Li, X., Li, B., Yu, X.Y., Wen, W.Q., Yao, J.Q.** A Continuous-wave Tunable Orange-red Source Based on Sum-frequency Generation in an Intra-cavity Periodically Poled LiNbO<sub>3</sub> Singly Resonant Optical Parametric Oscillator Cavity *Journal of Optics* 13 (9) 2011: pp. 1–5.  
<https://doi.org/10.1088/2040-8978/13/9/095201>
16. **Lin, J., Pask, H.M.** Nd:GdVO<sub>4</sub> self-Raman Laser Using Double-End Polarised Pumping at 880 nm for High Power Infrared and Visible Output *Applied Physics B* 108 (1) 2012: pp. 17–24.  
<https://doi.org/10.1007/S00340-012-5093-7>
17. **Zhu, P., Li, D.J., Hu, P.X., Schell, A., Shi, P., Haas, C.R., Wu, N.L., Du, K.M.** High Efficiency 165 W Near-diffraction-limited Nd:YVO<sub>4</sub> Slab Oscillator Pumped at 880 nm *Optics Letters* 33 (17) 2008: pp. 1930–1932.  
<https://doi.org/10.1364/OL.33.001930>
18. **Yu, Y.J., Chen, X.Y., Wang, C., Wu, C.T., Yu, M., Jin, G.Y.** High Repetition Rate 880 nm Diode-directly-pumped Electro-optic Q-switched Nd:GdVO<sub>4</sub> Laser with a Double-crystal RTP Electro-optic modulator *Optics Communications* 303 2013: pp. 39–42.  
<https://doi.org/10.1016/j.optcom.2013.04.023>
19. **Sato, Y., Taira, T., Pavel, N., Lupei, V.** Laser Operation with Near Quantum-defect Slope Efficiency in Nd:YVO<sub>4</sub> under Direct Pumping into the Emitting Level *Applied Physics Letters* 82 (6) 2003: pp. 844–847.  
<https://doi.org/10.1063/1.1544659>

19. **Sheng, Q., Liu, L., Ding, X., Jiang, P.B., Liu, J., Yu, X.Y., Wu, L., Zhang, G.Z., Zhao, C., Sun, B., Yao, J.Q.** Thermal Management of Nd:YVO<sub>4</sub> Laser by 808-/880-nm Dual-Wavelength Pumping *IEEE Photonics Journal* 9 (2) 2017: pp. 1–7.  
<https://doi.org/10.1109/JPHOT.2017.2672040>
20. **Huang, Y.J., Cho, H.H., Su, K.W., Chen, Y.F.** Dual-Wavelength Intracavity OPO with a Diffusion-Bonded Nd:YVO<sub>4</sub>/Nd: GdVO<sub>4</sub> Crystal *IEEE Photonics Technology Letters* 28 (10) 2016: pp. 1123–1126.  
<https://doi.org/10.1109/LPT.2016.2531906>
21. **Yang, H.K., Moon, B.K., Jeong, J.H.** Crystal Growth and luminescence Properties of the Nd: GdVO<sub>4</sub> Micro-rods: A Promising Laser Material *Ceramics International* 41 (5) 2015: pp. 7207–7210.  
<https://doi.org/10.1016/j.ceramint.2015.02.049>
22. **Sun, Y.X., Bai, Y., Li, D., Bai, B., Gong, Y.Z., Bai, J.T.** 946 nm Nd: YAG Double Q-switched Laser Based on Monolayer WSe<sub>2</sub> Saturable Absorber *Optics Express* 25 (18) 2017: pp. 21037–21048.  
<https://doi.org/10.1364/OE.25.021037>
23. **My, T.H., Robin, O., Mhibik, O., Drag, C., Bretenaker, F.** Stimulated Raman Scattering in an Optical Parametric Oscillator Based on Periodically Poled MgO-doped Stoichiometric LiTaO<sub>3</sub> *Optics Express* 17 (7) 2009: pp. 5912–5918.  
<https://doi.org/10.1364/OE.17.005912>



© Bai et al. 2020 Open Access This article is distributed under the terms of the Creative Commons Attribution 4.0 International License (<http://creativecommons.org/licenses/by/4.0/>), which permits unrestricted use, distribution, and reproduction in any medium, provided you give appropriate credit to the original author(s) and the source, provide a link to the Creative Commons license, and indicate if changes were made.